Journal of Anatomy

J. Anat. (2011) **219**, pp192–202 doi: 10.1111/j.1469-7580.2011.01384.x

The three-dimensional shape of serrations at barn owl wings: towards a typical natural serration as a role model for biomimetic applications

Thomas Bachmann[1] and Hermann Wagner[2]

[1]*Institute for Fluid Mechanics and Aerodynamics, TU Darmstadt, Darmstadt, Germany*
[2]*Institute for Biology 2, RWTH Aachen University, Aachen, Germany*

Abstract

Barn owl feathers at the leading edge of the wing are equipped with comb-like structures termed serrations on their outer vanes. Each serration is formed by one barb ending that separates and bends upwards. This structure is considered to play a role in air-flow control and noise reduction during flight. Hence, it has considerable potential for engineering applications, particularly in the aviation industry. Several publications have reported possible functions of serrations at artificial airfoils. However, only crude approximations of natural serrations have so far been investigated. We refer to these attempts as zero-order approximations of serrations. It was the goal of this study to present a quantitative three-dimensional characterization of natural serrations as first-order approximations (mean values) and second-order approximations (listed differences depending on the position of the serration along the leading edge). Confocal laser scanning microscopy was used for a three-dimensional reconstruction and investigation with high spatial resolution. Each serration was defined by its length, profile geometry and curvature. Furthermore, the orientation of the serrations at the leading edge was characterized by the inclination angle, the tilt angle and the separation distance of neighboring serrations. These data are discussed with respect to possible applications of serration-like structures for noise suppression and air-flow control.

Key words: aerodynamics; airflow; feather; flight; serration; transition.

Introduction

Members of the taxon *Strigiformes* (owls) have developed unique feather structures (Graham, 1934). Comb-like hooks termed serrations occur at the outer vanes of those feathers that build up the leading edge of the distal wing. Serrations are thought to influence the aerodynamic performance of the wing (Neuhaus et al. 1973; Ito, 2009) and to reduce flight noise (Kroeger et al. 1971; Neuhaus et al. 1973; Lilley, 1998). As such, serrations have attracted interest from engineers, and serration-like structures have been tested in rotor blades (Soderman, 1972) and at pantographs of high speed trains (Shinkansen, Japan; Benyus, 2002) to reduce airstream noise. Although the three-dimensional (3D) structure of the serration is important for its aerodynamic and noise reductive behavior, only crude two-dimensional models of serrations have so far been used in the above-mentioned applications. We shall refer to these efforts as zero-order approximations of serrations. It was the goal of this work to reconstruct the 3D shape of a typical natural serration. We call the result obtained from mean values a first-order approximation of a serration. A more detailed model, taking into account changes with the position on the wing, will yield a second-order approximation of a natural serration.

In an earlier work from our laboratory we characterized the morphometry of barn owl feathers on a macroscopic level (Bachmann et al. 2007). The vane of a feather is divided into an outer and inner part, each of which is made up of barbs (Bachmann et al. 2007). A barb consists of a central shaft from which hook and bow radiates originate. The hooklets on the hook radiates connect neighboring barbs, creating a closed vane.

In barn owls, serrations are formed by barbs of the 10th primary feather (Bachmann et al. 2007). Here, each serration is formed by the tip of a single barb. Hook and bow radiates originate from the shaft and function to form a closed vane and to support the shape of a serration. While

Correspondence
Thomas Bachmann, Institute for Fluid Mechanics and Aerodynamics, Technische Universität Darmstadt Flughafenstrasse 19, 64347 Griesheim, Germany. E: bachmann@sla.tu-darmstadt.de

Accepted for publication *29 March 2011*
Article published online *20 April 2011*

bow radiates are rather short and arise from the proximal barb side, hook radiates are longer and are located on the distal side of the barb shaft.

We divided barbs of the outer vane of the 10th primaries of barn owls into a proximal base and a distal tooth-shaped tip. The serration is the bent part of the barb (Bachmann et al. 2007). In the region of the serrations, hook and bow radiates decreased in length towards the barb tip and thereby supported the formation of the tooth-shape of the serration. Although the serrations were two-dimensionally described in Bachmann et al. (2007), a more detailed three-dimensional characterization has not been provided so far.

Three-dimensional specimen scans and surface reconstructions have become more and more important in describing the anatomy and morphology of natural structures. However, high-resolution scanning methods are often time-consuming and expensive when analyzing the whole object, not just the surface (Betz et al. 2007). Confocal laser scanning microscopy is a quick high-resolution imaging technique. Modern confocal laser scanning microscopes (CLSM) that are able to produce z-dependent image stacks may be used to investigate small-sized, (semi)translucent objects. Three-dimensional information can be extracted by scanning several layers of the specimen on the *z*-axis (Heuer & Loesel, 2009).

The objective of this paper is to derive a first- and second-order approximation of a serration to serve as a role model for engineering applications with the help of CLSM.

Materials and methods

Feather material

Six 10th primaries obtained from five barn owls (*Tyto alba pratincola*) of the colony from the Institute for Biology 2 (RWTH Aachen University, Germany) were investigated. Three feathers (two from a right wing, one from a left wing) were molted feathers and three feathers (two from a right wing, one from a left wing) were taken from wings of dead birds. All feathers were taken from specimens that had been used in other experiments under a permit from the local authorities (Landespräsidium für Natur, Umwelt und Verbraucherschutz Nordrhein, LANUV, Westfalen, Recklinghausen, Germany).

Digitizing of serrations

Serrations were obtained from single barbs at four different positions (20, 40, 60 and 80% length of vane) of six 10th primaries. The 24 barbs were cut at the rachis and fixed at the base to an object slide with polymer clay (Fimo classic; Staedtler Mars GmbH & Co. KG, Nuremberg, Germany) so that the barb tip pointed upwards.

A confocal laser scanning microscope (Leica TCS SP2; Leica Microsystems GmbH, Wetzlar, Germany) was used to scan and thus digitize the serrations. The auto-fluorescence of feather keratin was excited by applying a diode laser with a wavelength of 405 nm. Light emission was measured in different planes by progressing from the dorsal to the ventral direction. Out-of-focus light was eliminated by a spatial pinhole focal plane. As feather keratin is almost transparent, all structures become visible with this method. Spatial resolution was restricted to the specimen size and the lenses used here, $5.86 \times 5.86 \times 5$ μm per voxel. Due to the size of a serration, several scan series along the length of the serration were needed to cover the whole structure. The recorded images of each scan series were exported as image stacks in TIFF format. Three-dimensional models were assembled from these image stacks using the software AMIRA (Mercury Computer Systems GmbH, Berlin, Germany). In a next step, all surface reconstructions were superimposed manually with AMIRA to guarantee similar measurement positions within the serrations. In that way, cross-sections through the surfaces were always in the same distance from the beginning of the serration for all specimens.

As the serration is a three-dimensional object, we shall first define the coordinates as follows. The straight line along the barb shaft of the barb base is set to be the *y*-axis. The *x*-axis is defined to be perpendicular to the *y*-axis. It runs through the plane formed by the hook and the bow radiates. Finally, the *z*-axis lays perpendicular to the *x*-*y* plane (Fig. 1A).

Further analysis and morphometric measurements were done using AMIRA, CORELDRAW (Corel Corporation, Ottawa, Ontario, Canada) and MATLAB (The MathWorks Inc., Natick, MA, USA). The following parameters were obtained to characterize the three-dimensional shape of single serrations: length, thickness and width at different positions, proportion of hook to bow radiates in cross-section, and curvature. These parameters were measured as follows.

The length of each serration was determined by sampling the surface from the beginning of the curvature towards the barb tip using the 3D-line measure tool provided by AMIRA (Fig. 1B). For width and thickness measurements, the surface models were transversally cut perpendicular to the dorsal side (Fig. 1C). As the superposition of all serrations had an almost circular shape, a circle with a radius of 2150 μm was fitted onto the curvature. The center was placed above the beginning of the curvature, respectively the serration. Here, the first cross-sections were analyzed. Further cross-sections were made every 750 μm on the dorsal surface (Fig. 1C). Using this procedure, four cross-sections of each serration were made that yielded comparable information about width and thickness.

The width of the cross-section was the longest distance between the tips of the hook and bow radiates (Fig. 1D). The maximum thickness of the barb shaft served as an estimation of the maximum thickness of a serration (Fig. 1D). Each cross-section was further analyzed with respect to the ratio of hook to bow radiate width. To do so, the distance from the center of the barb shaft to either side (hook and bow radiates) were measured (Fig. 1D). Again, all distances were obtained using the 3D-line measure tool provided by AMIRA.

The curvature describes the bending of the serration to the dorsal side. Interestingly, 3D rotations of the surface models demonstrated no curvature in the *y*-axis within the serrations. Hence, the barb shaft resembled a more or less straight line by which the serration can be projected onto a 2D plane. Curvature measurements were performed in this plane, defined by the *y*- and *z*-axis. To do so, *z*-components were sampled every 250 μm in the *y*-direction using a measure grid designed with CORELDRAW (Fig. 1E). The resulting coordinates of the curvature were plotted and a fitting curve as a third-order polynomial was calculated.

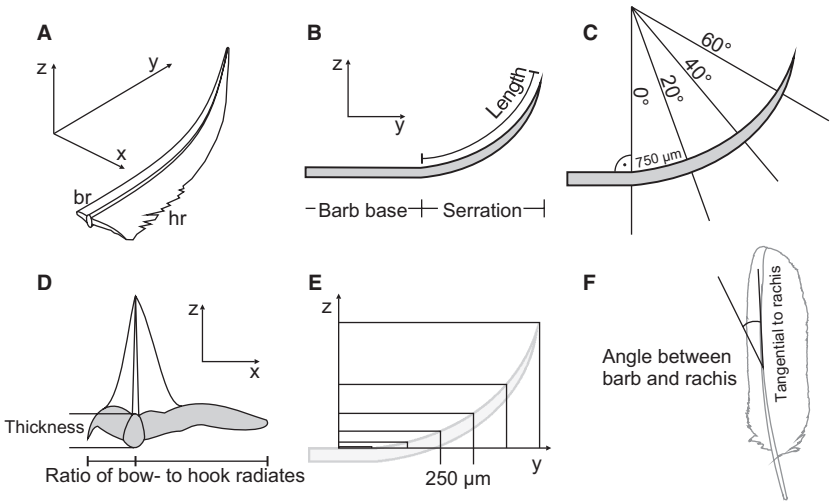

Fig. 1 Schematic drawings of the measuring specifications. (A) Definition of the axes within the serration. (B) Division of the base and the serration. The serration begins at the curvature of the barb shaft. Length measurements were performed at the dorsal surface. (C) Virtual profile sections perpendicular to the dorsal surface were analyzed every 750 μm. (D) Profiles were analyzed with respect to the thickness and the width of bow and hook radiates. Using the values of the width, the ratio of hook to bow radiates proportion was calculated. (E) The bending of each serration was sampled every 250 μm in the *y*-direction. (F) The angle between the barb shaft and the rachis was measured on photographs of 10th primaries.

Orientation of the serrations at the outer vane

Up to this point, separated serrations were considered. However, to characterize the orientation of serrations at the leading edge of the feather, further parameters had to be specified. The shaft of a serration is not perpendicularly attached to the leading edge, but at a given angle. As the base of barbs at the leading edge is straight, the inclination of the serrations to the leading edge of the feather was measured as the angle between the barb shaft and the rachis. These angles were obtained from dorsal photographs of 10th primaries of the barn owl (Fig. 1F).

As the 10th primary has varying orientations during flight, one exemplary position during gliding flight was taken to measure the orientation of the leading edge towards the flight path of the owl. The angle between the tangential line and the flight path was measured at a 3D reconstruction of a wing surface of one barn owl during gliding flight (Wolf et al. 2010). Furthermore, each serration was tilted towards the leading edge of the feather. This tilt angle was determined under visual control using a stereomicroscope.

Finally, the distance between the serrations was measured by counting the number of barbs per centimeter vane length at the four sampling areas of the 10th primary (20, 40, 60 and 80% length of vane). The local distance was determined by dividing 1 cm by the number of barbs.

Results

In the barn owl the leading edge of the distal wing is formed by the outer vane of the 10th primary. The vane itself consists of many interlinked barbs. The barbs can interlink via tiny hooklets of the hook radiates (distal) that cling to grooves of the bow radiates (proximal) of adjacent barbs. The hook radiates terminate into filament-like structures called pennula. In owls, these pennula are extremely elongated (Bachmann et al. 2007) (Fig. 2).

In the 10th primary, the tips of barbs of the outer vane form serrations at their endings (Fig. 2). For further analysis and a precise nomenclature, we divided barbs of the outer vane into two parts: the base and the serration (Figs 1B and 2E). The bases interconnect to a closed vane, whereas the serrations are separated and form curved tooth-shaped tips.

We further distinguished between the shape of a single serration and the orientation of an array of serrations at the leading edge of the 10th primary. A single serration had a complex 3D shape characterized by the profile sections, a taper towards the tip, and a bending towards the dorsal side. Each profile (perpendicular to the surface) was defined by the thickness, the width and the position of the central shaft and thus the proportion of the depth of hook to bow radiates.

In the following, we first describe the morphometry of single natural serrations, then we define the orientation of each serration at the leading edge of the feather. First- and second-order approximations of the serrations are presented.

For a quantitative description of single serrations, 24 separated serrations of six different 10th primaries of the barn owl were digitized and reconstructed. Figure 3 displays polygon meshes of all investigated serrations in an isometrical view. The serrations differed in length and tip appearance depending on the position measured. Some serrations ended in an acute tip, others in a more rounded tip. Serrations of distal parts of the feather (80%) had rounded tips and were the shortest (1823 μm ± SD of 239), in contrast to serrations at basal parts of the feather, which had acute tips (20%) and

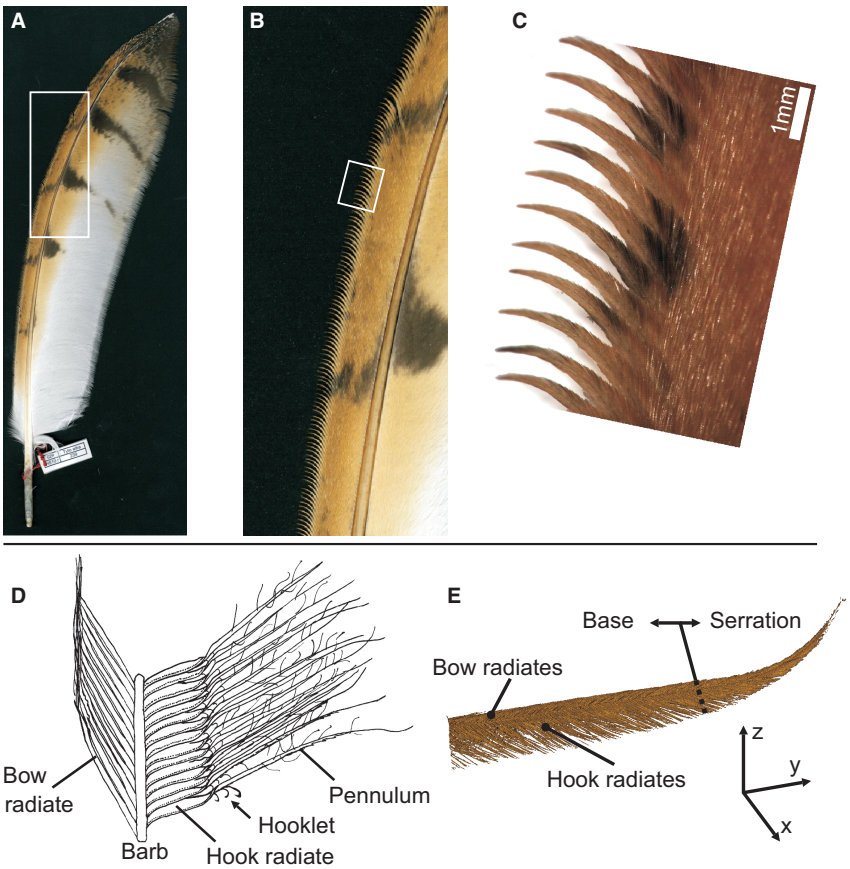

Fig. 2 Serrations of the 10th primary of a barn owl. (A) Photograph of a 10th primary of a barn owl. (B,C) Barb endings of the outer vane form serrations by their tips. (D) Schematic of the anatomy of a barb. (E) Three-dimensional reconstruction of a serration (polygon mesh).

were statistically significantly longer (2470 μm ± 383 SD) (*t*-test, $P = 0.0057$). Serrations located in central regions of the feather were the longest (2669 μm ± 337 SD) (Table 1) and also exhibited acute tips (Fig. 3).

All serrations tapered towards their tip in an almost linear way. The smallest mean width at the beginning of the curvature (528 μm ± 122 SD) (Table 1) was found in serrations of basal feather parts. Serrations of distal feather parts (60% length of vane) were statistically significantly wider (683 μm ± 68 SD) (*t*-test, $P = 0.0218$) (Table 1).

In cross-section, the position of the central shaft and thus the origin of the hook and bow radiates was approximately at 30% serration width for all serrations measured (0.28–0.33) (Table 1). The only exception was found at the tips of serrations from the 20 and 40% length of vane. Here, the position of the central shaft was shifted slightly towards the center (0.35–0.41) (Table 1). In general, the hook radiates had a much greater influence on the width than the bow radiates. This unequal distribution of the bow and hook radiates width resulted in an asymmetrical appearance of the profiles and thus an asymmetrical appearance of a single serration. Elongated pennula were responsible for the larger width of the hook radiates (Fig. 2D).

All serrations were curved to the dorsal side. Interestingly, only small differences were found between the curvatures of the serrations. As no curvature was observed in the *x*-*z* plane, we projected and measured the curvature on the *y*-*z* plane. Sampling the curvature with a given *y*-value of 250 μm enabled us to compare the curvature of different serrations. Figure 4 shows the data points of the serrations investigated grouped by their origin. The curvature was almost the same for all serrations. All data points of the same *y*-component were compared statistically in a Levene's test. Statistical differences occurred only in a comparison of all serrations (Levene's statistic: 4.4444; df 10,242; *P*-value = 0) (Table 2). No statistical differences were found when comparing serrations of the same position within a feather ($P = 0.02458$–0.13726) (Table 2). A fitting curve, a third-order polynomial [$f_{position(y)} = ay^3 + by^2 + cy$], characterized the curvature of a typical serration at each feather position (Fig. 4). Although the curvatures of serrations of different positions were statistically diverse, differences were quite small.

Up to this point we characterized the shape of single serrations of different sample locations at the leading edge of the 10th primary. However, the orientation of each serration at the outer vane had to be specified. As all serrations

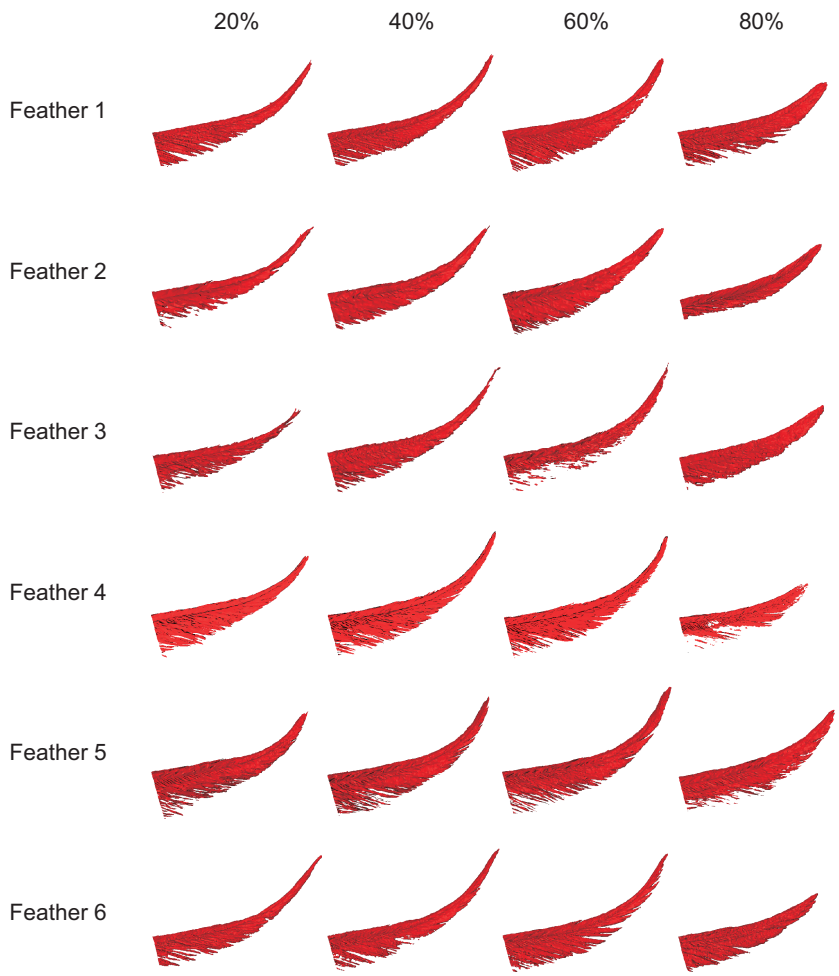

Fig. 3 Surface reconstruction (polygon meshes, artificial colors) of the 24 serrations investigated (isometrical view). The columns reflect the different feathers; the rows depict the different positions of the serrations at the outer vane (% length of vane). Note: Serrations of the two left feathers four and five were mirrored for a better comparison.

are oriented in a line, three parameters define the orientation of each serration at the leading edge: the distance, the angle of the shaft towards the leading edge, and the tilt angle of the serration towards the anterior side. The distance of the serrations was measured as the distance from the central shafts. The smallest distances were measured at basal parts of the feather (493 μm ± 26 SD at 20% length of vane) and the largest distances at distal parts (671 μm ± 68 SD at 80% length of vane) (Table 1). As the basal width of the serrations is related to the tip distance, the arrangement of the serrations was different within the feather as well.

The inclination angle varied depending on the position of the serration measured. The largest angles were measured at 20% length of vane (31.5°, 5.1 SD) and the smallest at 80% length of vane (24.7°, 1.7 SD) (Table 1). This finding was statistically significant (*t*-test, $P = 0.0432$). By contrast, the tilt angle was almost constant throughout the leading edge. The overall mean tilt angle was 36.1° ± 1.2 SD (Table 1). No statistical differences were found concerning this parameter at any position measured.

The rachis of the 10th primary of the barn owl was curved, resulting in different leading edge angles towards the free stream direction (Fig. 1F). Hence, different angles of the serration towards the free stream direction occurred as well. We reconstructed these angles for one special case, the gliding flight of the owl. Quantitative data of angles between the serrations and the rachis were combined with angular measurements of the leading edge towards the free stream direction at a 1D–3D reconstructed wing of a gliding barn owl. In the central regions of the feather the inclination angle of the serrations was almost perpendicular to the air flow (82–91°). Serrations pointed towards the air flow (74°) at basal parts of the feather, whereas they bent away from the air flow at distal parts (113°) (Table 1).

First-order approximation

We based our first-order approximation of serrations (Fig. 5) on geometrical data of natural serrations of the barn owl located at central regions (40–60%) of the feather.

Table 1 Morphometric parameters (mean ± SD) of serrations of barn owl 10th primaries at four different positions along the outer vane (20–80%).

	20%	40%	60%	80%
Length (μm)	2470 ± 383	2622 ± 369	2716 ± 328	1823 ± 239
Thickness (μm)				
at 0 μm	87.2 ± 6.9	86.6 ± 10.7	85.4 ± 12.6	82.0 ± 15.1
at 750 μm	84.0 ± 9.8	81.0 ± 11.3	75.0 ± 14.0	77.2 ± 18.1
at 1500 μm	78.3 ± 10.3	77.9 ± 12.1	62.5 ± 10.2	73.9 ± 10.4
at 2250 μm	53.9 ± n = 1	56.8 ± 16.9	46.9 ± 8.6	
Width (μm)				
at 0 μm	528.3 ± 122.3	601.9 ± 82.6	683.2 ± 67.6	652.3 ± 97.7
at 750 μm	355.9 ± 83.5	471.0 ± 69.9	504.9 ± 47.5	643.4 ± 95.6
at 1500 μm	206.5 ± 105.9	323.1 ± 43.8	341.8 + /- 29.4	194.6 ± 159.7
at 2250 μm	157.2 ± 21.1	179.1 + /- 45.9	181.6 ± 44.7	215.7 ± n = 1
Ratio of br/h				
at 0 μm	0.30 ± 0.04	0.30 ± 0.04	0.29 ± 0.02	0.28 ± 0.04
at 750 μm	0.33 ± 0.03	0.33 ± 0.03	0.33 ± 0.03	0.32 ± 0.04
at 1500 μm	0.42 ± 0.04	0.36 ± 0.05	0.31 ± 0.02	0.32 ± 0.04
Angle shaft/LE	31.5° ± 5.1	30.4° ± 2.1	28.5° ± 1.4	24.7° ± 1.7
Tilt angle (°) n = 4	36.7 ± 0.8	35.3 ± 1.3	36.2 ± 1.4	36.3 ± 1.2
Angle LE/flight path (n = 1)	106°	112°	120°	138°
Angle serration/flight path	74.5°	81.6°	91.5°	113.3°
Angle of LE to freestream	106°	112°	120°	138°
Angle of serration to freestream	74°	82°	91°	113°
In gliding flight, n = 1				

n = 6. A detailed description of the variables can be found in Fig. 1 and the relevant subsection.
hr, hook radiates; br, bow radiates; LE, leading edge.

Below, we describe the shape and geometry of a single serration, and then specify the orientation of an array of serrations at a leading edge of an airfoil.

A single serration may be described by its length, curvature and profile distribution. For technical serrations we propose a smooth surface and elliptically shaped profiles (perpendicular to the upper surface), resulting in a smooth serration (Fig. 5). Whereas the basal width of the serration at the beginning of the curvature was 640 μm, it decreased linearly towards the tip, characterized by the formula:

$$f_{\text{width}} = -0.2067y + 640$$

The tip of serrations of the first-order approximation was slightly rounded because the point $f_{\text{width}} = 0$ was further away than the serration length itself (2670 μm; Table 3). The profiles are asymmetrically shaped with the maximum thickness located at 0.3 width of the profile. The thickness (perpendicular to the surface) decreased almost linearly from 86 μm (11 SD) at the beginning of the curvature towards 52 μm (14 SD) at 2250 μm, which can be expressed by the following formula:

$$f_{\text{thickness}} = -0.0149y + 86$$

Such a tapered beam is curved in z-direction. A third-order polynomial, given by the following formula, describes this curvature:

$$f_{\text{curvature}}(y) = 8\text{E-}08y^3 - 6\text{E-}05y^2 + 0.1154y.$$

For an array of serrations, further parameters were necessary to ensure a functional orientation. The y-axis of the serration was not attached at right angles to the leading edge, but at an angle of 29°. Furthermore, serrations were tilted towards the anterior side. The tilt angle of the y-z-plane was 36°. To ensure a symmetrical orientation of the serrations, the tip distance should equal the distance from the basal central shafts (575 μm). Table 3 summarizes the geometrical description of the first-order approximation.

Second-order approximation

Our second-order approximation advances beyond the characterization of one typical serration. As the wing of a barn owl is curved in the distal half and all serrations are attached to this curved part, different orientations and lengths of serrations were observed. The second-order approximation takes these differences into account.

As mentioned for the first-order approximation, we propose a smooth surface and elliptically shaped profiles for all artificial serrations. Differences in curvature and thickness distribution were quite small when serrations of different positions were compared (Table 4).

Although all serrations were equally shaped in principle, some parameters differed depending on the position of the serration at the leading edge. The serrations became longer (2470–2720 μm) from 20 to 60% length of vane, whereas

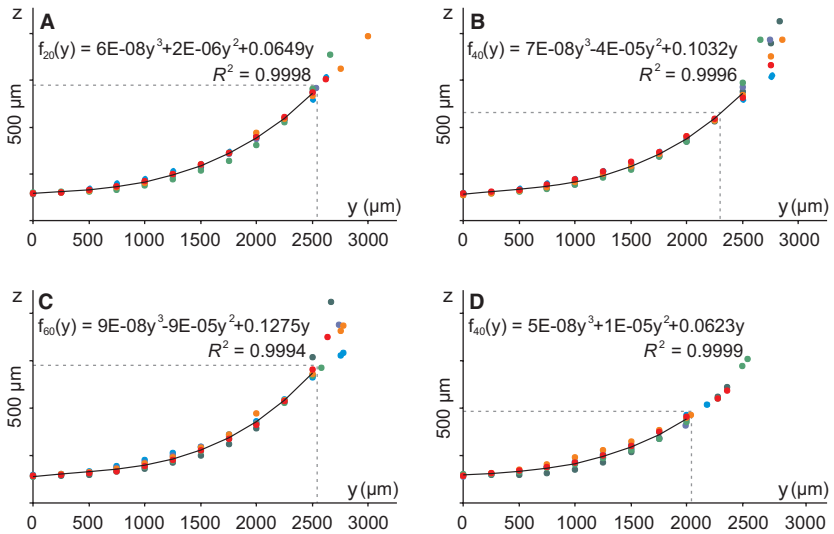

Fig. 4 Curvatures of serrations of different positions within the feather. The four panels represent the four sampling areas of the 10th primary: A = 20% B = 40% C = 60% and D = 80% length of vane. The different colors represent individual serrations of each position. The black line indicates a fitting curve of those data points that showed no statistical difference. The relations and accuracies (R^2) are given in each diagram. Curve shapes within the dotted horizontal and vertical lines are not statistically diverse (Levene's test, see Table 2).

Table 2 Statistical analysis of the curvature of the serrations at different positions along the outer vanes of barn owl's 10th primaries (% length of vane).

Serration position	All	At 20%	At 40%	At 60%	At 80%
Levene's statistic	4.4444	2.1929	2.38839	1.58738	1.66005
Degrees of freedom	10, 242	10, 52	9, 50	10, 51	10, 53
P-value	0	0.03287	0.02458	0.13726	0.11527

the shortest serrations (1820 μm) were located at the tip of the feather (Table 4). Width values were approximated by a linear function in dependency of the length of the serration. Also in that case, the width increased within 20–60% length of vane and slightly decreased towards the tip of the feather. The formulas expressed the tip appearance by inserting the total length of the particular serration. Furthermore, the width values were related to the distance of the serration at the leading edge. Small basal widths (500 μm) were associated with small distances (490 μm) at the feather's base and larger basal widths (650 μm) with larger distances of the serrations (670 μm) at the tip of the feather (Table 4).

Under static conditions with no external aerodynamic forces acting on the feather, the inclination angles of the serrations towards the leading edge decreased with the smaller ones at the tip of the feather. As mentioned before, the 10th primary of the barn owl was curved. Hence, the serrations were oriented at different angles to the chordwise direction of the fixed, sprawled-out wing. Whereas the serrations pointed towards the direction of potential air

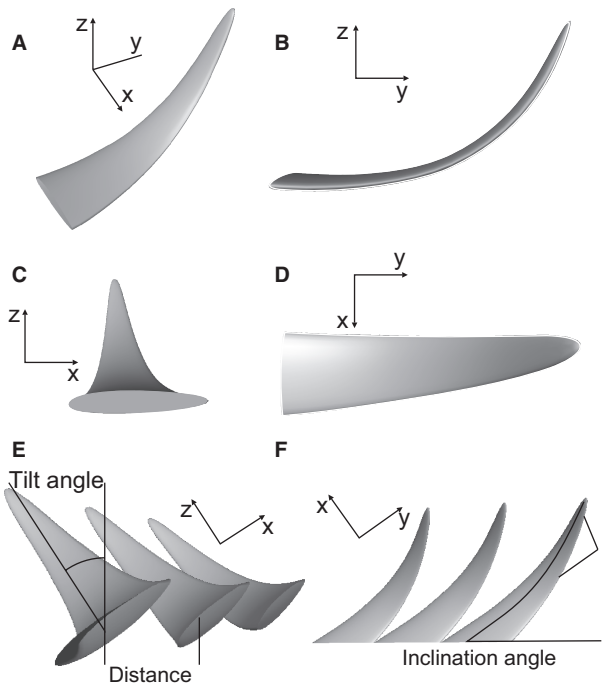

Fig. 5 Schematic of a first-order approximation of a serration in different views (A–D). (E) Tilt angle and distance. (F) Inclination angle towards the leading edge of a wing.

flow at proximal regions of the wing, they bent away from that direction at distal parts. The reconstructed angles are listed in Table 4. However, note that these data were obtained under static conditions. They may differ significantly in free flight conditions and different flight modes due to the bending behavior of the feathers.

Table 3 Geometrical data of the first-order approximation of a barn owl's serration. Length, width and thickness describe the shape of a single serration; distance and the different angulations characterize their orientation at the leading edge. A detailed description of the variables can be found in Fig. 1 and in the relevant subsection.

Single serration	
Length	2670 μm
Width (in dependence of length)	$f_{width} = -0.2067y + 640$ ($R^2 = 1$)
Thickness (in dependence of length)	$f_{thickness} = -0.0149y + 86$ ($R^2 = 0.963$)
Position of maximum thickness	0.3 width
Array of serrations	
Distance	575 μm
Angle serration/leading edge	29°
Angle serration/flight path ($n = 1$)	87°
Tilt angle	36°

The chord of the wing decreased towards the tip due to the curvature of the 10th primary and tapering of the wing. We calculated the chord of barn owl wings using published data from Nachtigall & Klimbingat (1985). The chord was 0.36 length of wing at the base of the 10th primary, but only 0.08 length of wing at the tip.

The last parameter for a defined position of the serrations at the leading edge is the tilt angle. No differences in the tilt angle were found under static conditions. Hence, we propose a constant tilt angle of all serrations at the leading edge of 36° towards the base of the wing. However, we would like to stress again that the orientation of the serrations measured at a resting feather is different to their functional state in free flight. In free flight, the 10th primary is supposed to bend under aerodynamic loads. Although the primaries of barn owls do not bend as much as those of a flying stork (Rüppell, 1980), the effect on the tilt angle might be significant.

Discussion

In barn owls, the leading edge of the distal wing is formed by the 10th primary remex. The outer vane of this feather carries serrations. Barb endings separate and bow to the dorsal side, logically changing their form and function. Even though some publications deal with descriptions of the serrations (Graham, 1934; Neuhaus et al. 1973; Hersh et al. 1974; Taylor, 1994; Lilley, 1998; Mebs & Scherzinger, 2000; Bachmann et al. 2007; Ito, 2009), none has provided quantitative three-dimensional information of this filigreed and complex structure.

Table 4 Geometrical data of the second-order approximation of barn owls' serrations.

	20%	40%	60%	80%
Single serration				
Length (μm)	2470	2620	2720	1820
Width (in dependency of the length)	$x = -0.1684y + 501$	$x = -0.1888y + 606$	$x = -0.2224y + 678$	$x = -0.2552y + 649$
Accuracy	$R^2 = 0.9512$	$R^2 = 0.9994$	$R^2 = 0.9994$	$R^2 = 0.9887$
Thickness (in dependency of the length)	$z = -9E\text{-}06y^2 + 0.0071y + 86.39$	$z = -7E\text{-}06y^2 + 0.0032y + 85.575$	$z = -0.0171y + 86.65$	$z = -0.0054y + 81.75$
Accuracy	$R^2 = 0.9808$	$R^2 = 0.9587$	$R^2 = 0.9918$	$R^2 = 0.9887$
Position of t_{max} (dependent on the length)	$x = 5E\text{-}08y^2 + 2E\text{-}06y + 0.2992$	$x = 9E\text{-}09y^2 + 2E\text{-}05y + 0.3048$	$x = -5E\text{-}08y^2 + 9E\text{-}05y + 0.2873$	$x = -3E\text{-}08y^2 + 7E\text{-}05y + 0.2832$
Accuracy	$R^2 = 1$	$R^2 = 1$	$R^2 = 1$	$R^2 = 1$
Curvature (dependent on y)	$z = 6E\text{-}08y3 + 2E\text{-}06y2 + 0.0649y$	$z = 7E\text{-}08y^3 - 4E\text{-}05y^2 + 0.1032y$	$z = 9E\text{-}08y^3 - 9E\text{-}05y^2 + 0.1275y$	$z = 5E\text{-}08y^3 + 1E\text{-}^{05y2} + 0.0623y$
Accuracy	$R^2 = 0.9998$	$R^2 = 0.9996$	$R^2 = 0.9994$	$R^2 = 0.9999$
Array of serrations				
Distance (μm)	490	560	590	670
Inclination angle	32°	30°	29°	25°
Tilt angle	36°	36°	36°	36°
Angle of LE to freestream direction	106°	112°	120°	138°
Angle of serration to freestream direction	74°	82°	91°	113°
In gliding flight $N = 1$				

A detailed description of the variables can be found in Fig. 1 and the relevant subsection.
LE, leading edge.

In this study, we used confocal laser scanning microscopy to reconstruct and measure serrations of the outer vane of the barn owl 10th primaries. This method yielded high resolution data of the geometry and the shape of serrations. We characterized serrations of four different positions of the outer vane anatomically by their length, cross-sectional geometry and curvature. Furthermore, the orientation of each serration at the leading edge of the wing was determined by measuring the distance, the inclination angle and the tilt angle. This three-dimensional information was used to present first- and second-order approximations of serrations that advance beyond the geometry of artificial serrations as used so far for technical applications.

Functional aspects of serrations

Functionally, serrations are thought to influence the aerodynamic performance of the wing (Neuhaus et al. 1973; Ito, 2009) and to reduce flight noise (Kroeger et al. 1971; Neuhaus et al. 1973; Lilley, 1998). Both theories have been investigated in the past by engineers and biologists.

In aviation, serrations might act as turbulence generators at the leading edge of the wing. In a series of papers from the early 1970s (Arndt & Nagel, 1972; Soderman, 1972; Neuhaus et al. 1973; Schwind & Allen, 1973; Hersh et al. 1974) several wind tunnel experiments were performed to investigate the impact of artificial two-dimensional serrations of different length and spacing on the flow field. In these studies, serrations influenced the air flow separation, enhanced lift of the wings, and reduced noise generated by the wings. Such parameters are important for owls, especially during hunting flight and striking. However, it is questionable whether the results of the above-mentioned experiments are applicable to the flight of barn owls, as the Reynold's number differs significantly within the experiments and in comparison with the flight of owls. Barn owls fly in the Reynold's number range of 8×10^4–1.5×10^5 in contrast to airfoils from Soderman (1972), for instance, which were measured in the Reynold's number range of 1.03×10^6 to 2.32×10^6.

In a more biological approach to understanding the function of serrations, Neuhaus et al. (1973) performed experiments with tawny owls (*Strix aluco*) and mallard ducks (*Anas platyrhynchos*). These authors showed that serrations act as a transition strip and thereby stabilize the air flow around the wing. Furthermore, Neuhaus et al. (1973) speculated that the serrations reduce noise at high angles of attack which is normally found at critical flight maneuvers such as landing, take-off or striking.

However, the artificial serrations in the studies of Arndt & Nagel (1972), Hersh et al. (1974), Neuhaus et al. (1973), Schwind & Allen (1973), and Soderman (1972) cannot be compared with those of owls. For a more biomimetic approach to understanding the mechanisms owls do make use of, a scalable description of the natural model is needed. In the following, we will first discuss the geometry of natural serrations investigated at barn owl wings and then conclude with our first- and second-order approximation of serrations as a role model for technical applications.

Natural serrations at barn owl wings

Barn owls are nocturnal birds of prey which detect and locate prey using acoustic information. Hence, they need to fly silently. The silent flight is achieved by an almost laminar air flow around the wing (Neuhaus et al. 1973). Large, noisy vortices on the wing surface are efficiently prevented.

Barn owl wings differ from those of other birds and aircraft (Nachtigall & Klimbingat, 1985). The distal wing of barn owls resembles a slightly cambered plate (Nachtigall & Klimbingat, 1985) over which the airflow normally tends to separate, especially at low-speed flight (Roskam & Lan, 1997). Serrations at the leading edge prevent a separation and increase the lift by generating a turbulent boundary layer over the airfoil upper surface (Ito, 2009). The turbulent boundary layer delays leading- and trailing-edge flow separation to higher angles of attack (Ito, 2009) similarly as shown in experiments by Soderman (1972) at higher Reynold's numbers.

As mentioned above, Neuhaus et al. (1973) showed that serrations influence the noise generation only at steep angles of attack. One explanation might be that in cruise flight conditions the stagnation point at the leading edge results in a relative low air flow through the serrations due to the low air stream velocity. At sharp angles of attack, however, serrations comb through the air like a plough through a field. By their bending and orientation, serrations induce tiny vortices running over the dorsal wing surface as shown by Ito (2009). This phenomenon increases the lift and reduces the noise of barn owl wings during flapping flight and striking, which is extremely useful for the owl.

The distal wing of the barn owl tapers towards the tip. Additionally, higher velocities and angles of attack occur at this wing part in flight, especially in flapping flight (Rüppell, 1980). Consequently, serrations have to be differently sized and oriented along the leading edge to maintain a constant excitation of the air flow. Proximal serrations have to induce the boundary layer of larger chord sections than distal serrations at the wing tip. This can be seen in a different spacing and length of the natural serrations. Furthermore, the tip appearance varies between proximal and distal serrations. As all serrations taper similarly towards their tip, shorter serrations from the distal feather part have more rounded tips. Those of basal and central regions have acute tips.

The orientation of the serrations towards the flight path is dependent on three angular parameters: (1) the inclination angle of the bases towards the rachis, (2) the curvature of the rachis itself and (3) the orientation of the

rachis towards the flight path. The inclination angle and the curvature are easily measured at separated feathers. However, the orientation of the feather within the wing during flight is hard to measure. We were able to estimate these parameters from a 3D reconstruction of one wing of a barn owl during gliding flight and the accompanying flight path. Interestingly, all serrations were oriented at more or less right angles (90.2° ± SD of 16.9) to the flight path in this special case. With this knowledge, the orientation of serrations in artificial wings can be fitted to match that in barn owl flight. This is a great advantage compared with earlier attempts, but we would like to note here that our proposal is so far based on only one special case of flight mode, the gliding flight. The orientation may vary significantly in different flight modes, as wing planform and angle of attack are highly dynamic during flight (Norberg, 2002; Lentink et al. 2007).

First-order and second-order approximations

The proposed approximations of natural serrations are based on quantitative morphometric data of serrations found at barn owl 10th primaries. The mean values of the characterizing parameters were taken to describe the shape, size and inclination of serrations at the leading edge of the wing. However, some parameters, for instance the parallel orientation of hook and bow radiates, were neglected because we believed that these structures are the result of evolutionary and developmental processes and, due to their size, may not have an aerodynamic relevance. The surface textures of the serrations are relatively small in terms of the serration and the wing. Hence, our first-order and second-order approximations have smooth surfaces and elliptic-like cross-sectional profiles.

While the first-order approximation describes a mean serration of medial feather regions, the second-order approximation advances beyond this simplified characterization. Here, wing specific parameters were taken into consideration. Small spacing of the serrations and acute tips are related to larger wing chords of 0.31–0.36 length of wing (Nachtigall & Klimbingat, 1985). By contrast, rounded tips and small serrations with a wider spacing are related to the wing tip with a wing chord of approximately 0.08 length of wing (Nachtigall & Klimbingat, 1985). For a biomimetic application, these parameters have to be adjusted for each particular wing of interest.

In this study we propose technical approximations of serrations that may now be used to understand the mechanisms owls make use of in more detail, for instance with flow visualization techniques in wind, water or oil tunnels. The understanding of these phenomena and the transformation to higher Reynold's numbers could lead to applications for safer and less noisy wings in the aviation industry.

Acknowledgement

We are indebted to Dr. Rudi Loesel for advice about confocal laser scanning microscopy and to Sandra Brill for support during the statistical analysis. We thank Thomas Wolf from the DLR Göttingen and Alexander Friedl from the Universität der Bundeswehr Munich for providing three-dimensional data of barn owl wings from free flight experiments. Financial support was provided by the German Research Foundation (WA606/15-2 within SPP1207).

Conflict of interests

The authors declare that they have no competing interests.

Author contributions

All authors conceived of and designed the research. T.B. performed all measurements and reconstructions and drafted the manuscript. H.W. supervised the study and was involved in drafting the manuscript. Both authors read and approved the final manuscript.

References

Arndt R, Nagel T (1972) Effect of leading edge serrations on noise radiation from a model rotor. *AAIA Paper* 655.

Bachmann T, Klän S, Baumgartner W, et al. (2007) Morphometric characterisation of wing feathers of the barn owl (*Tyto alba pratincola*) and the pigeon (*Columba livia*). *Front Zool* **4**, 23.

Benyus JM (2002) *Innovation Inspired by Nature*. New York: Perennial.

Betz O, Wegst U, Weide D, et al. (2007) Imaging applications of synchrotron X-ray phase contrast microtomography in biological morphology and biomaterials science. I. General aspects of the technique and its advantages in the analysis of millimetre-sized arthropod structure. *J Microsc* **227**, 51–72.

Graham R (1934) The silent flight of owls. *J Roy Aero Soc* **38**, 837–843.

Hersh A, Soderman P, Hayden R (1974) Investigation of acoustic effects of leading-edge serrations on airfoils. *J Aircr* **11**, 197–202.

Heuer C, Loesel R (2009) Three-dimensional reconstruction of mushroom body neuropils in the polychaete species *Nereis diversicolor* and *Harmothoe areolata* (Phylodocida, Annelida). *Zoomorph* **128**, 219–226.

Ito S (2009) Aerodynamic influence of leading-edge serrations on an airfoil in a low Reynold's number – A study of an owl wing with leading-edge serrations. *J Biomech Sci Engin* **4**, 117–123.

Kroeger R, Gruschka H, Helvey T (1971) Low speed aerodynamics for ultraquiet flight. *AFFDL* **71–75**, 1–55.

Lentink D, Müller UK, Stamhuis EJ, et al. (2007) How swifts control their glide performance with morphing wings. *Nature* **446**, 1082–1085.

Lilley G (1998) A study of the silent flight of the owl. AIAA Paper 98, 2340.

Mebs T, Scherzinger W (2000) *Die Eulen Europas*. Stuttgart: Franckh-Kosmos Verlag.

Nachtigall W, Klimbingat A (1985) Messungen der Flügelgeometrie mit der Profilkamm-Methode und geometrische Flügelkennzeichnung einheimischer Eulen. In *Biona Report 3* (ed. Nachtigall W), pp. 45–68. Stuttgart: Gustav Fischer Verlag.

Neuhaus W, Bretting H, Schweizer B (1973) Morphologische und funktionelle Untersuchungen über den lautlosen Flug der Eule (*Strix aluco*) im Vergleich zum Flug der Ente (*Anas plathyrhynchos*). *Biol Zentr Bl* **92**, 495–512.

Norberg U (2002) Structure, form, and function of flight in engineering and the living world. *J Morph* **252**, 52–81.

Roskam J, Lan C-T (1997) *Airplane Aerodynamics and Performanc*e. Lawrence: Design, analysis and research cooperation.

Rüppell G (1980) *Vogelflug*. Hamburg: Rowohlt Taschenbuch Verlag.

Schwind R, Allen H (1973) The effects of leading-edge serrations on reducing flow unsteadiness about airfoils. AIAA paper 1973, 89.

Soderman P (1972) Aerodynamic effects of leading-edge serrations on a two-dimensional airfoil. *NASA Tech Memo* **X**, 2643.

Taylor I (1994) *Barn Owls: Predator–Prey Relationship and Conservation*. Cambridge: Cambridge University Press.

Wolf T, Kirmse T, Konrath R, et al. (2010) Measuring shape of bird wings during flight using an optical correlation based method, 14th Int Symp on Flow Vis (ISFV), Daegu, Korea.